Supporting information for:

Enhancement of the intrinsic light harvesting capacity of $Cs_2AgBiBr_6$ double perovskite *via* modification with sulphide

Narendra Pai[a,b], Jianfeng Lu[b,c], Mingchao Wang[d], Anthony S. R. Chesman[e,f], Aaron Seeber[e], Pavel V. Cherepanov[a], Dimuthu C. Senevirathna[a], Thomas R. Gengenbach[e], Nikhil V. Medhekar[d], Philip C. Andrews[a], Udo Bach[b,c,e,f] and Alexandr N. Simonov[a,g,*]

[a] School of Chemistry, Monash University, Clayton, Victoria 3800, Australia
[b] ARC Centre of Excellence for Exciton Science, Monash University, Clayton, Victoria 3800, Australia
[c] Department of Chemical Engineering, Monash University, Clayton, Victoria 3800, Australia
[d] Department of Materials Science and Engineering, Monash University, Clayton, Victoria 3800, Australia
[e] Commonwealth Scientific and Industrial Research Organisation Manufacturing, Clayton, Victoria 3168, Australia
[f] Melbourne Centre for Nanofabrication, Clayton, Victoria 3168, Australia
[g] ARC Centre of Excellence for Electromaterials Science, Monash University, Clayton, Victoria 3800, Australia

E-mail: alexandr.simonov@monash.edu

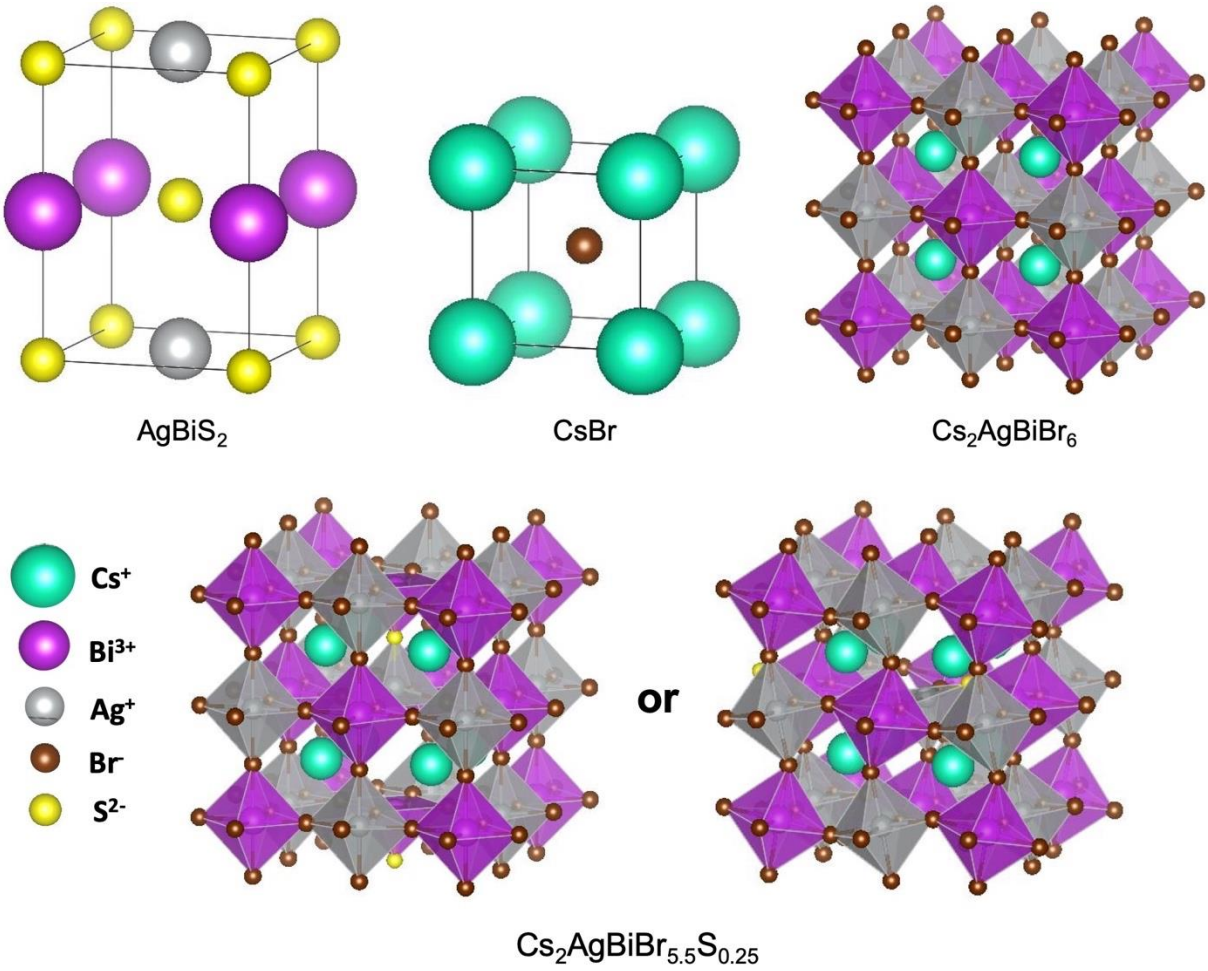

Figure S1. Crystal structures of relaxed $AgBiS_2$, CsBr, $Cs_2AgBiBr_6$, and $Cs_2AgBiBr_{6-2x}S_x$ unit cells calculated by replacing far-edge (left) or adjacent edge (right) bromide atoms with S^{2-}.

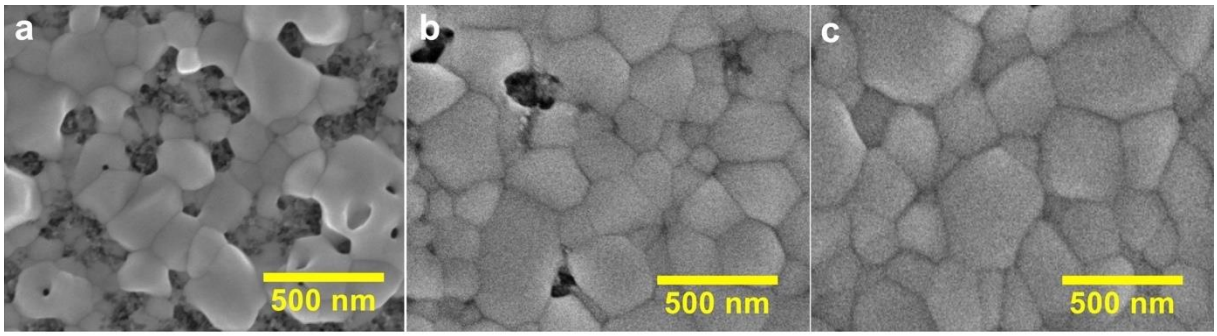

Figure S2. Top-view SEM images of the $Cs_2AgBiBr_6$ films coated onto m-TiO_2|c-TiO_2|FTO *via* (a) conventional spin-coating (2500 rpm for 30 s) and (b-c) two-step spin-coating (500 rpm for 10 s; 2500 rpm for 30 s) followed by (a-b) placing the sample on a hot-plate pre-heated to 280 °C for 10 min or (c) ramping the temperature of the sample at 0.5 ° s^{-1} to 280 °C, and keeping at this temperature for 10 min.

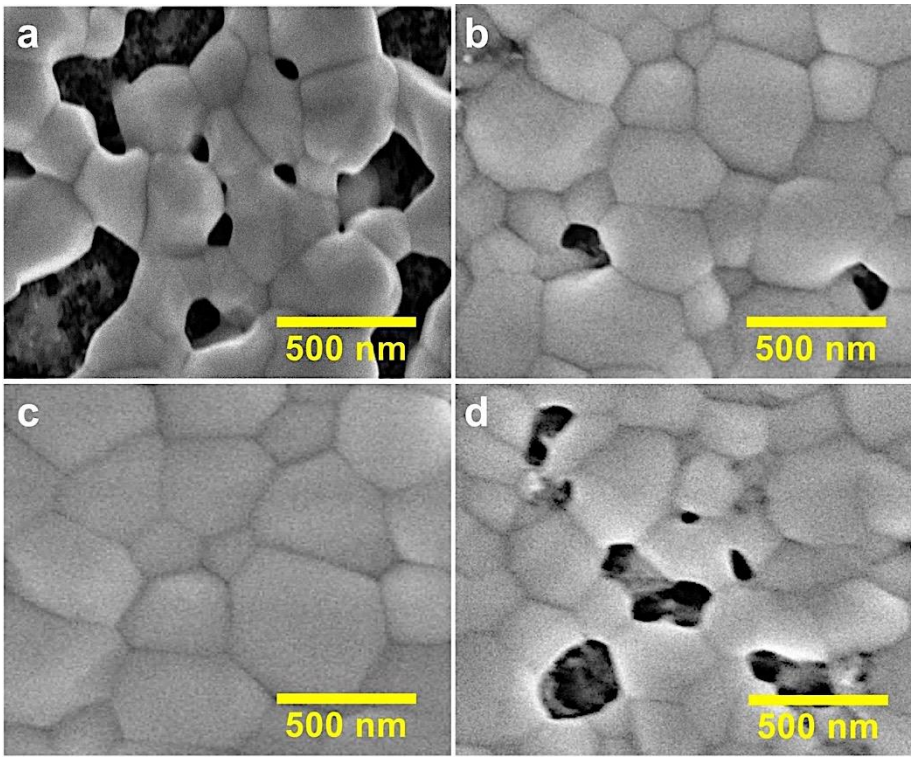

Figure S3. Top-view SEM images of $Cs_2AgBiBr_6$ films prepared using different precursor concentrations: (a) 0.40, (b) 0.50, (c) 0.55, and (d) 0.60 M. Deposition onto m-TiO_2|c-TiO_2|FTO supports was undertaken *via* a two-step spin-coating followed by heating on a hot plate at 280 °C (slow ramping at 0.5 °C s^{-1}), and maintaining this temperature for 10 min.

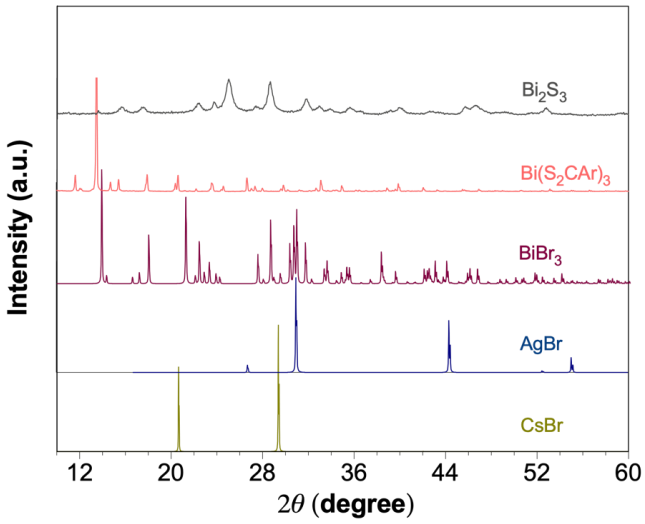

Figure S4. XRD patterns of Bi_2S_3 obtained by annealing $Bi(S_2CAr)_3$ at 150 °C (*grey*), $Bi(S_2CAr)_3$ (*pink*), $BiBr_3$ (*maroon*), AgBr (*blue*), and CsBr (*dark tan*).

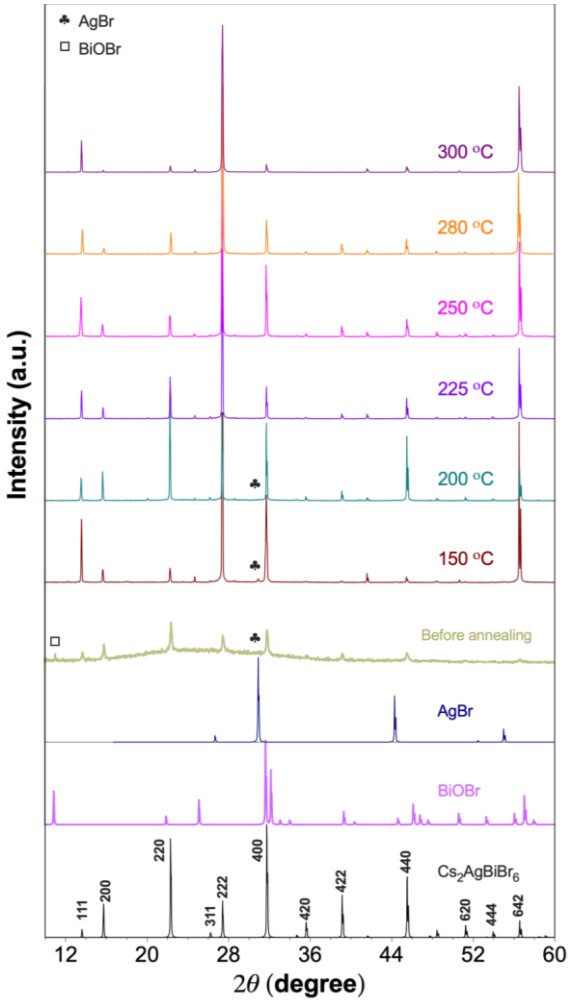

Figure S5. XRD patterns of materials obtained by two step spin-coating of the 0.55 M [CsBr + AgBr + $BiBr_6$] precursor solution and subseqeunt annealing at 150 (*dark red*), 200 (*teal*), 225 (*purple*), 250 (*magenta*), 280 (*orange*) and 300 °C (*plum*) for 10 min (heat ramp 5 °C s^{-1}). Data for the sample that was not annealed are shown as *tan* curve. Tabulated diffractograms for $Cs_2AgBiBr_6$ (*black*, JCPDS 01-084-8699), AgBr (*dark blue*, JCPDS 00-006-0438) and BiOBr (*light purple*, JCPDS 00-052-0084) are shown for reference.

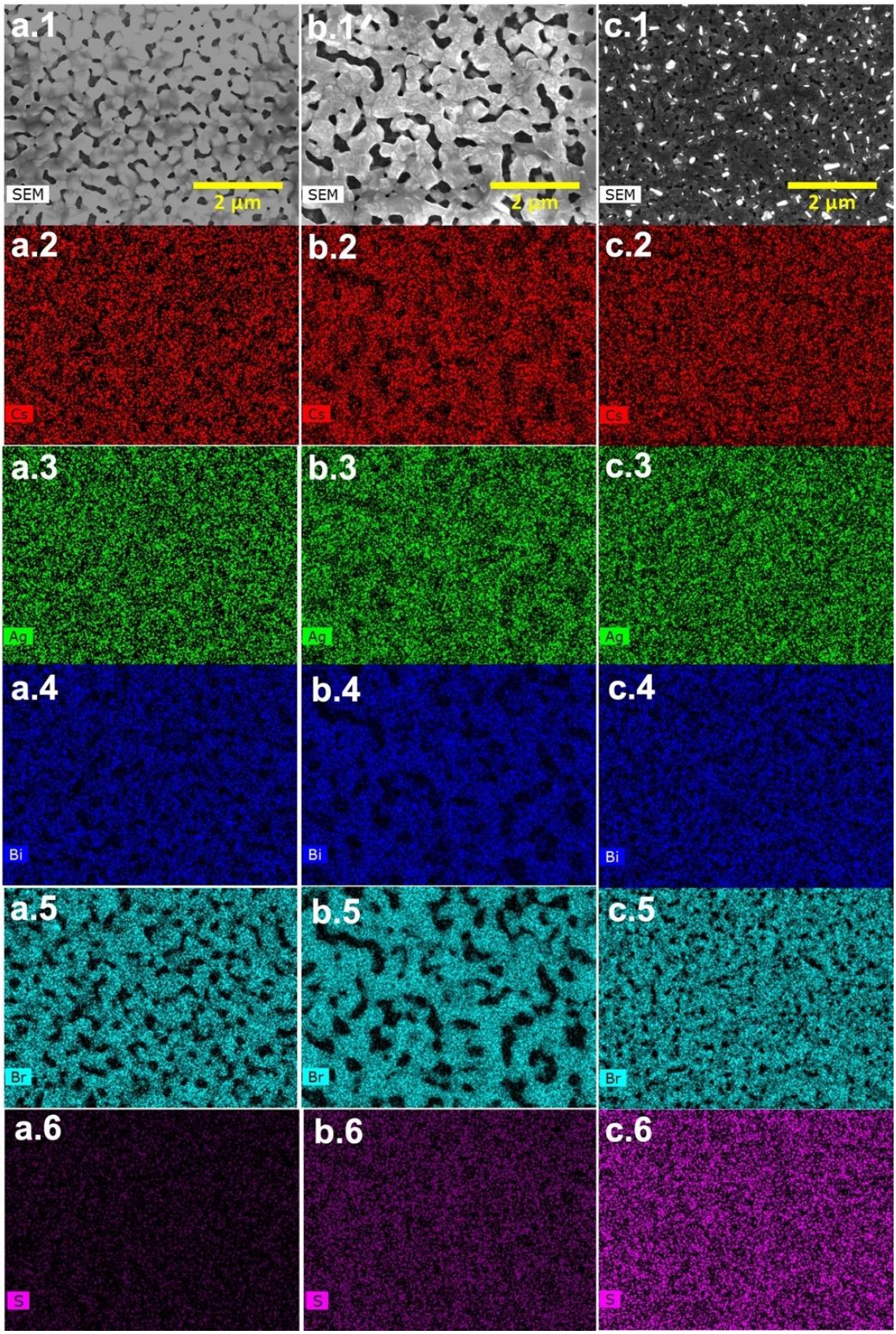

Figure S6. SEM images and corresponding energy dispersive X-ray elemental maps for (a) $Cs_2AgBiBr_6$, (b) $Cs_2AgBiBr_{5.6}S_{0.2}$ and (c) $Cs_2AgBiBr_4S$ films deposited onto glass supports.

Table S1. Composition[a] of $Cs_2AgBiBr_{6-2x}S_x$ films[b] according to the EDX/SEM mapping analysis.[c]

x	Cs	Ag	Bi	Br	S
0.00	2.14 ± 0.12	1.02 ± 0.01	1	8.2 ± 0.2	0.01 ± 0.01
0.05	2.14 ± 0.10	1.02 ± 0.02	1	8.1 ± 0.2	0.06 ± 0.03
0.10	2.16 ± 0.11	1.03 ± 0.03	1	7.96 ± 0.13	0.12 ± 0.03
0.15	2.14 ± 0.13	1.02 ± 0.02	1	7.76 ± 0.14	0.16 ± 0.02
0.20	2.12 ± 0.11	1.01 ± 0.02	1	7.7 ± 0.2	0.23 ± 0.03
0.50	2.16 ± 0.11	1.03 ± 0.03	1	7.20 ± 0.13	0.55 ± 0.05
1.0	2.13 ± 0.12	1.01 ± 0.02	1	3.54 ± 0.13	1.2 ± 0.1
2.0	2.16 ± 0.12	1.03 ± 0.04	1	3.4 ± 0.2	2.3 ± 0.1

[a] Normalised with respect to bismuth concentration; average and one standard deviation data for at least three samples of each type are shown. [b] Films deposited onto glass support were analysed directly. [c] Data are exemplified in Figure S6.

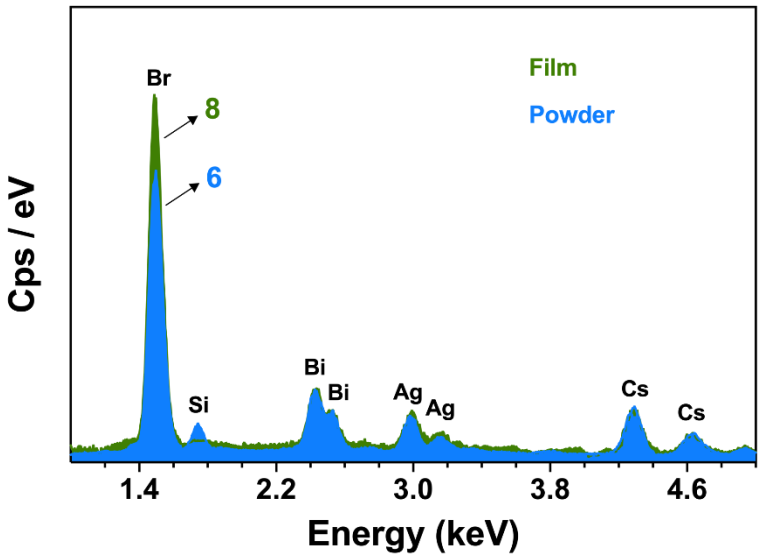

Figure S7. EDX spectra of a $CS_2AgBiBr_6$ film deposited onto glass (*green*) and of the powder obtained by scratching off the same film (*blue*).

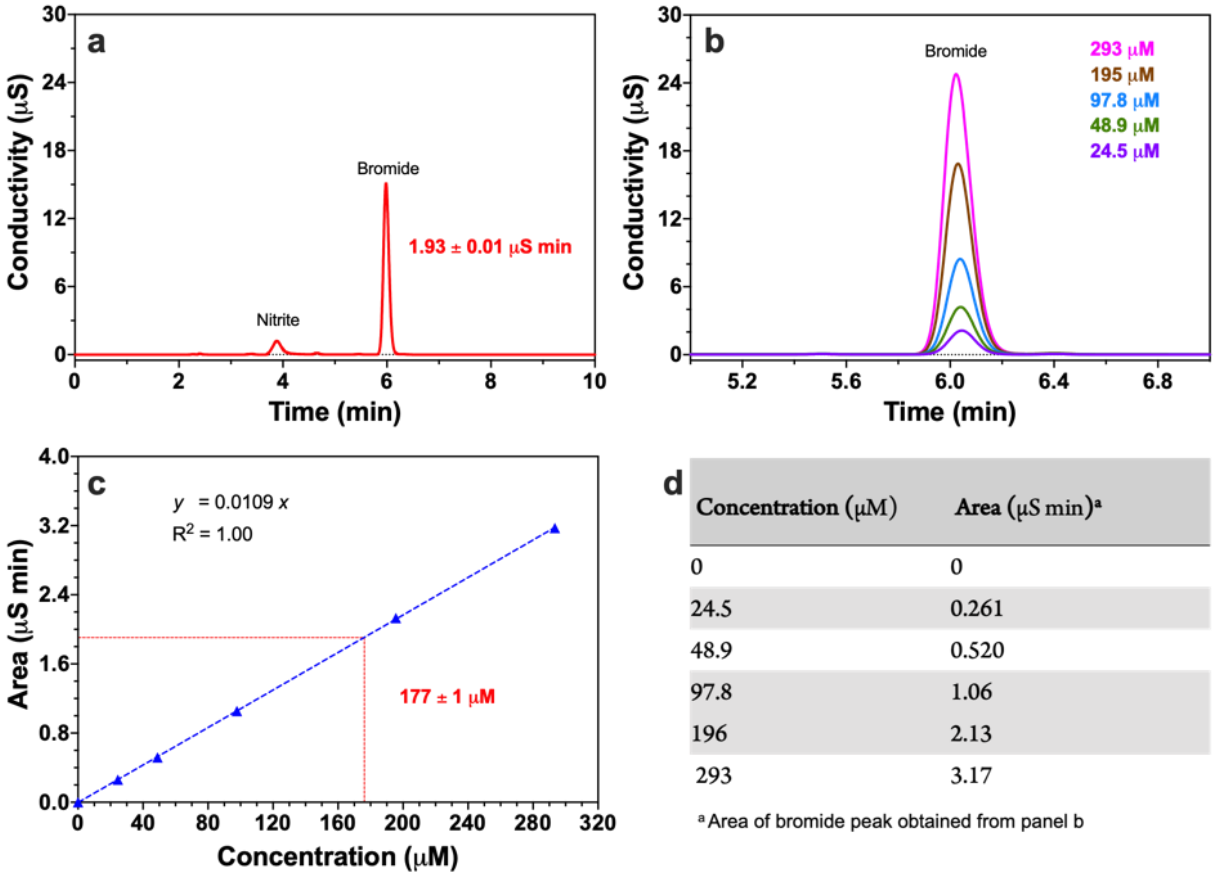

d

Concentration (μM)	Area (μS min)[a]
0	0
24.5	0.261
48.9	0.520
97.8	1.06
196	2.13
293	3.17

[a] Area of bromide peak obtained from panel b

Figure S8. Ion chromatographic analysis of bromide in $Cs_2AgBiBr_6$. Total ion chromatogram obtained by dissolving (a) 3.8 mg of $Cs_2AgBiBr_6$ and (b) NaBr (concentrations: 24.5 (*purple*), 48.9 (*green*), 97.8 (*light blue*), 196 (*brown*), and 293 μM (*magenta*)) in 10 mL of 0.01 M aqueous KOH. (c) Calibration curve (*dashed* line is a linear approximation), and (d) area of the bromide peak for NaBr standard solutions (experimental data shown in panel b). Area corresponding to the bromide peak is provided in panel a, and the corresponding concentration is shown in panel c with *dotted* lines.

Supplementary information for the ion chromatographic analysis:

Dissolution reaction	$Cs_2AgBiBr_6 \rightarrow 2\ Cs^+ + AgBr_{(s)}\downarrow + Bi^{3+} + 5\ Br^-$
Sample mass	$m_{sample} = 3.8 \times 10^{-3}$ g
Sample volume	$V_{sample} = 0.01$ L
Area of bromide peak	$A = 1.93 \pm 0.01$ μS min
Slope of the calibration plot	$s = 0.0109 \times 10^{-6}$ M μS^{-1} min^{-1}
Concentration of Br^-	$c_{Br} = 177 \pm 1 \times 10^{-6}$ M
Considering AgBr precipitation, x is calculated as	$x = \dfrac{1 + \frac{c_{Br} M_{Cs_2AgBi} V_{sample}}{m_{sample}}}{1 - \frac{c_{Br} M_{Br} V_{sample}}{m_{sample}}}$

where M_{Cs_2AgBi} is the molecular weight of Cs_2AgBi, and M_{Br} is the molecular weight of Br.

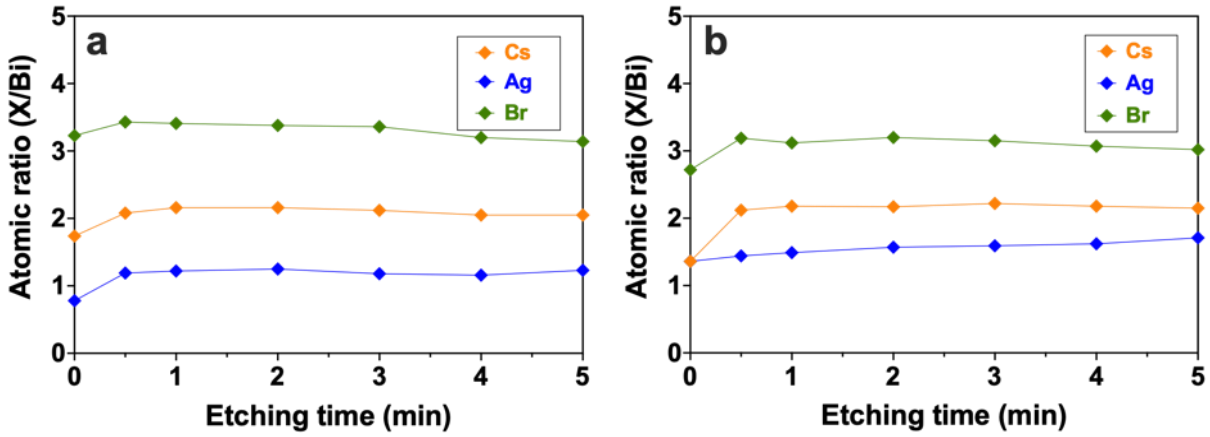

Figure S9. Distribution of caesium (*orange*), bismuth (*blue*) and bromine (*green*) (shown as atomic ratio with respect to bismuth) in (a) $Cs_2AgBiBr_6$, and (b) $Cs_2AgBiBr_{5.8}S_{0.1}$ films deposited onto FTO supports derived from XPS depth profiling analysis. Significant amount of tin was detected after 5 min of Ar etching.

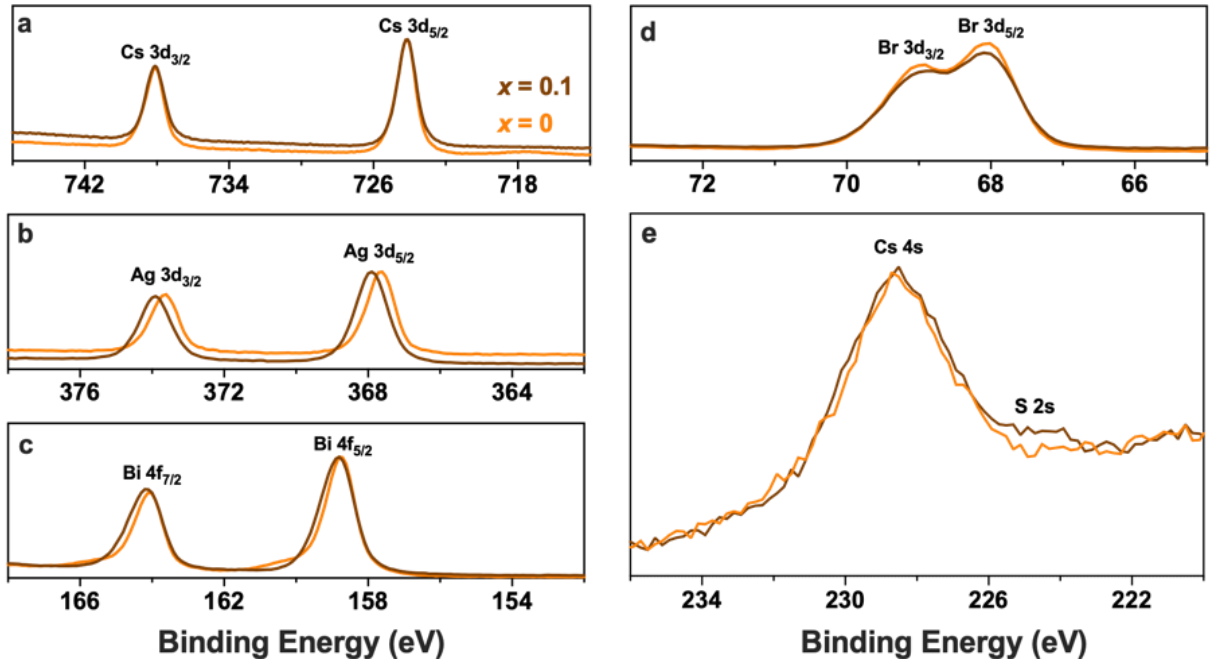

Figure S10. (a) Cs 3d, (b) Ag 3d, (c) Bi 4f, (d) Br 3d and (e) Cs 4s + S 2s spectra of $Cs_2AgBiBr_{6-2x}S_x$ with $x = 0$ (*orange*) and 0.10 (*brown*). Samples were prepared by spin-coating precursor solutions onto flat FTO supports and annealing at 280 °C for 10 min.

Table S2. Lattice parameters obtained by the refinement of the XRD data for the $Cs_2AgBiBr_{6-2x}S_x$ films with low amount of sulphur.

x	Space group	Lattice parameters[a]				
		a (Å)	c (Å)	α (°)	β (°)	γ (°)
0	F-3m	11.2697 ± 0.0003	11.2697 ± 0.0003	90	90	90
0.05	F-3m	11.2671 ± 0.0006	11.2671 ± 0.0006	90	90	90
0.10	F-3m	11.2678 ± 0.0003	11.2678 ± 0.0003	90	90	90
0.15	F-3m	11.2671 ± 0.0009	11.2671 ± 0.0009	90	90	90
0.20	F-3m	11.2656 ± 0.0009	11.2656 ± 0.0009	90	90	90

[a] Derived from the TOPAS fitting of the crystallographic data as those exemplified in Figure 2 (main text).

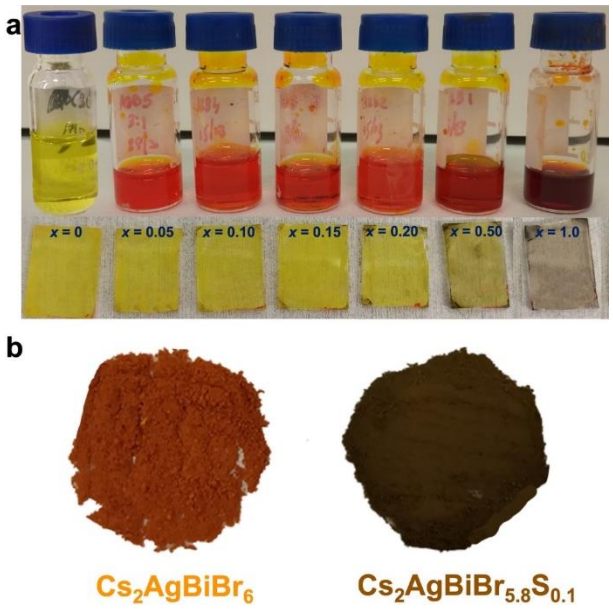

Figure S11. Photographs of (a) the 0.55 M [CsBr + AgBr + $BiBr_3$] precursor solutions in DMSO, and the resulting films produced *via* spin-coating onto glass substrates followed by annealing at 280 °C; (b) powders synthesised *via* annealing precursors drop-casted on glass substrates at 280 °C.

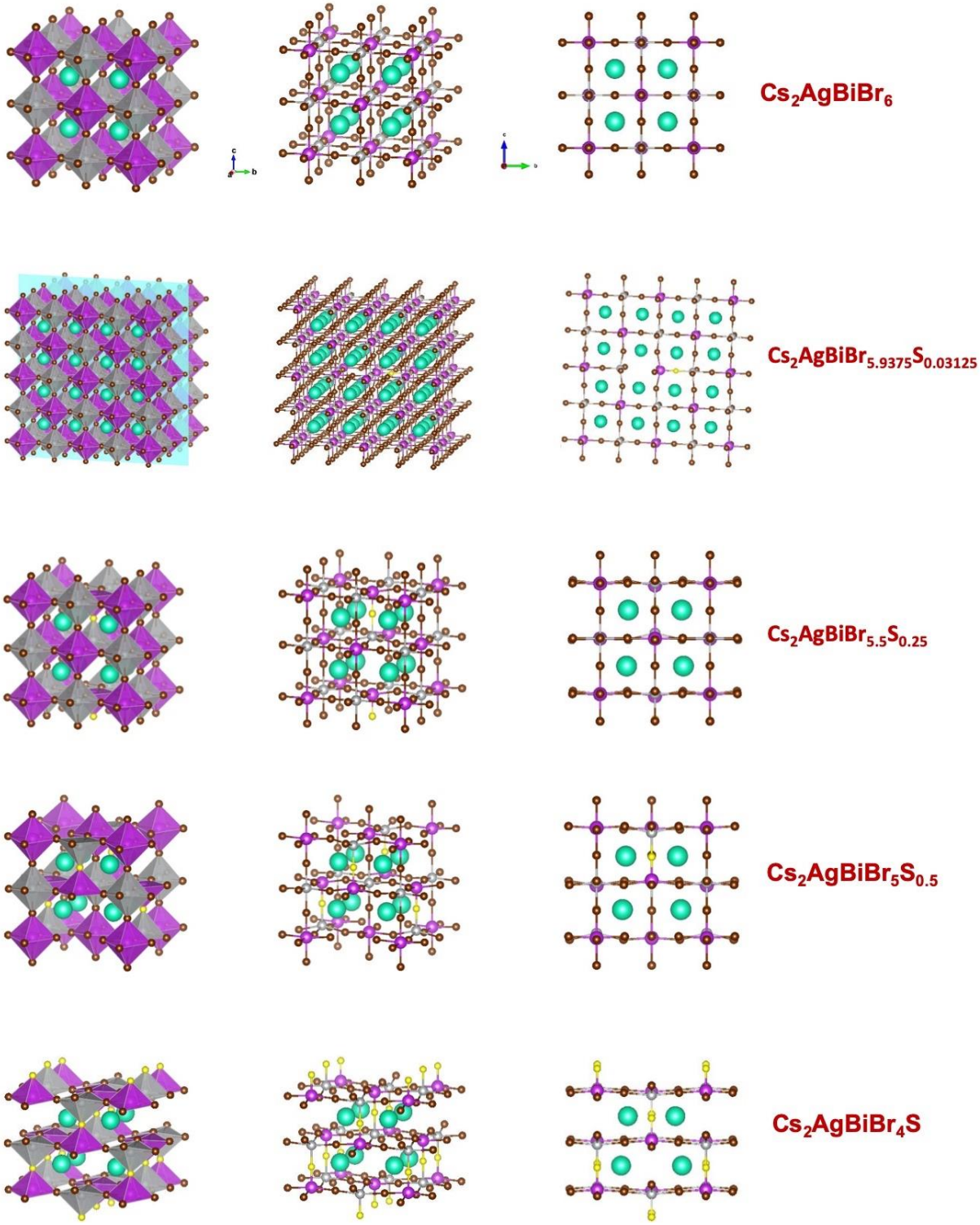

Figure S12. Possible crystallographical changes induced by replacing far edge bromides with divalent sulphide at different ratio.

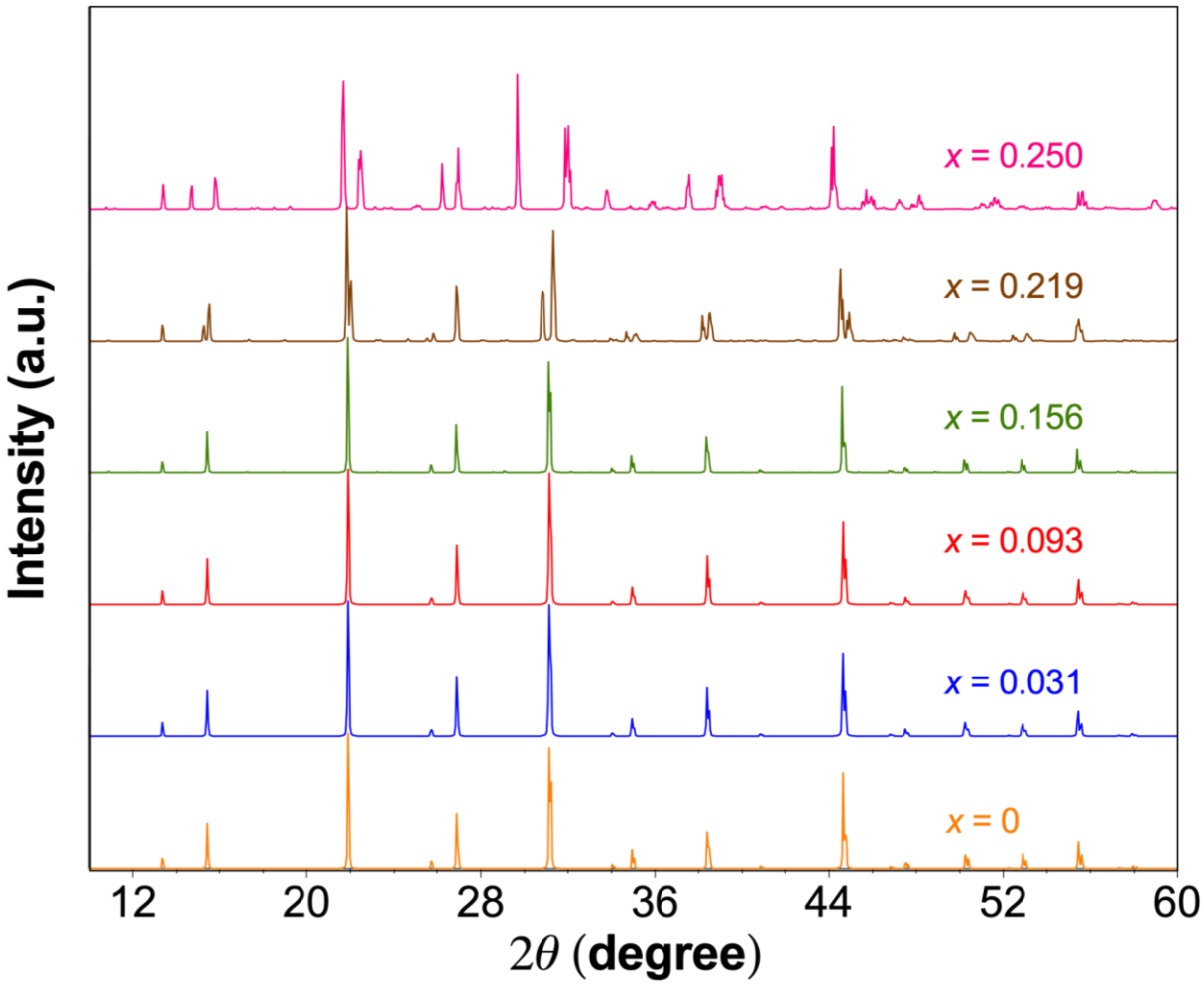

Figure S13. Simulated diffraction patterns of the possible relaxed crystal structures obtained *via* replacing far edge bromides with divalent sulphide at different ratio.

Table S3. Theoreticall lattice parameters for modelled $Cs_2AgBiBr_{6-2x}S_x$ relaxed structures at 0 K.

x	Space group	Lattice parameters[a]				
		a (Å)	c (Å)	*α* (°)	*β* (°)	*γ* (°)
0	F-3m	11.4775	11.4775	90	90	90
0.031	F-3m	11.4593	11.4593	90	90	90
0.093	F-3m	11.4693	11.4693	90	90	90
0.156	F-3m	11.4693	11.4693	90	90	90
0.218	F-3m	11.4693	11.4693	90	90	90

Table S4. Calculated ΔH_D, ΔS and ΔG_D (at 298 K) for $Cs_2AgBiBr_{6-2x}S_x$ per unit cell.

Parameter (meV)	Bromine positions replaced	*x* 0.031	0.093	0.16	0.22	0.25	0.5	1.0
ΔH_D	Adjacent	-3.58	-26.8	-66.3	-115	-133	-346	-397
	Far-edge	0.688	-15.8	-41.4	-68.1	-81.6	-158	-177
ΔS	Adjacent	-0.0164	-0.0357	-0.0489	-0.0588	-0.0628	-0.0788	-0.0601
	Far-edge	-0.0164	-0.0357	-0.0489	-0.0588	-0.0628	-0.0788	-0.0601
ΔG_D	Adjacent	1.30	-16.2	-51.7	-97.9	-115	-322	-379
	Far-edge	5.57	-5.15	-26.8	-50.6	-62.9	-135	-159

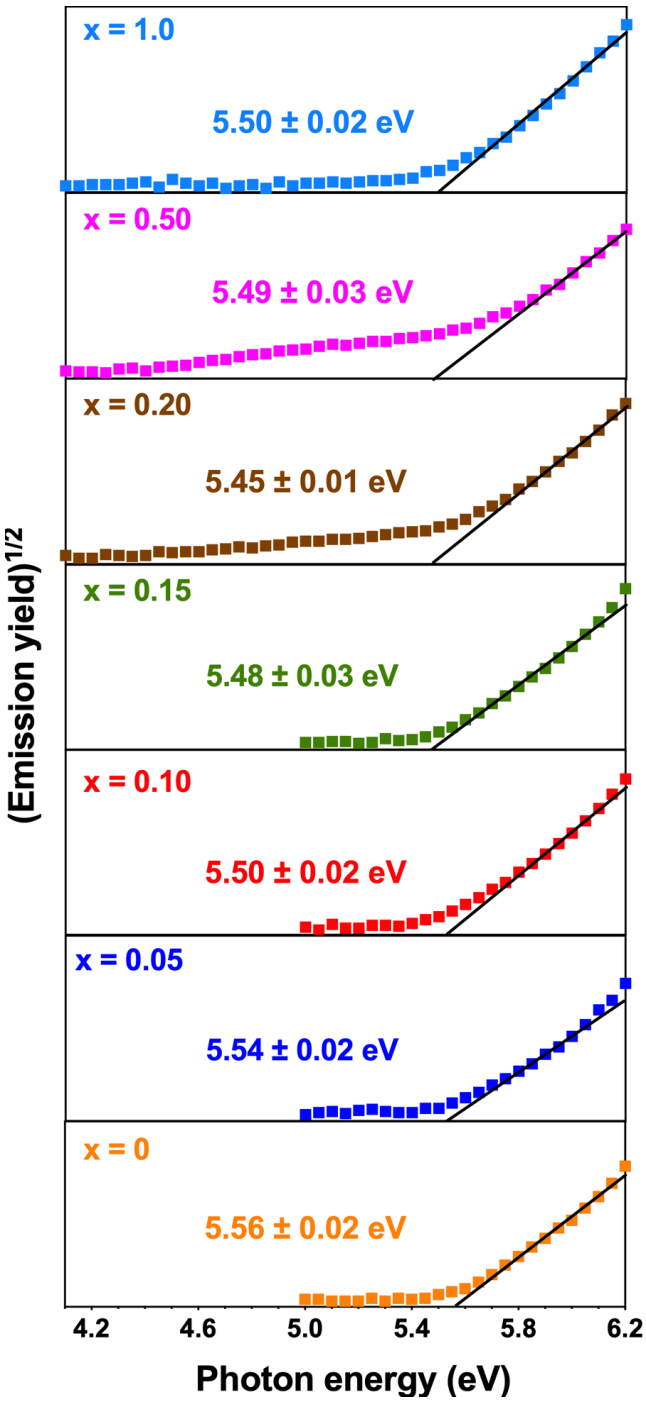

Figure S14. PESA data acquired for $Cs_2AgBiBr_{6-2x}S_x$ films deposited onto c-TiO_2|FTO substrates with $x = 0$ (*orange*), 0.05 (*blue*), 0.1 (*red*), 0.15 (*green*), 0.2 (*brown*), 0.5 (*magenta*), and 1.0 (*light blue*). *Black* lines exemplify linear fits used to determine the E_{VB} values, which are shown in the plots as mean ± one standard deviation derived from the characterisation of at least 3 independent samples of each type. Early onsets of absorption for samples $x = 0.2$ and 0.5 are attributed to impurity phases present on the surface of the films (as supported by Figure 2) and are not considered in the calculation of E_{VB}.

Table S5. Photovoltaic parameters[a] of the Au|spiro-OMeTAD|$Cs_2AgBiBr_{6-2x}S_x$ + m-TiO_2|c-TiO_2|FTO solar cells (aperture 0.16 cm^2) under simulated 1 sun AM1.5G irradiation.

x (at.%)		V_{oc} (mV)	J_{sc} (mA cm^{-2})	FF (%)	PCE (%)	qSPO (%) [b]
0	Average [c]	1010 ± 10	2.1 ± 0.2	64.0 ± 0.4	1.3 ± 0.1	1.3 ± 0.1
	Best [d]	1020	2.1	64.2	1.4	1.4
0.05	Average [c]	960 ± 20	2.2 ± 0.2	64.3 ± 0.3	1.4 ± 0.1	1.3 ± 0.2
	Best [d]	980	2.4	64.4	1.5	1.6
0.10	Average [c]	910 ± 20	3.0 ± 0.3	65.0 ± 0.4	1.8 ± 0.1	1.9 ± 0.1
	Best [d]	930	3.2	65.2	1.9	2.0
0.15	Average [c]	830 ± 20	2.8 ± 0.2	66.0 ± 0.4	1.6 ± 0.1	1.4 ± 0.3
	Best [d]	850	3.0	66.5	1.7	1.8
0.20	Average [c]	780 ± 10	1.9 ± 0.3	63.7 ± 0.5	1.0 ± 0.1	0.7 ± 0.3
	Best [d]	790	2.2	64.3	1.1	1.1
0.50	Average [c]	750 ± 10	0.9 ± 0.2	68.2 ± 0.2	0.45 ± 0.07	0.3 ± 0.2
	Best [d]	760	1.0	68.3	0.55	0.5
1.0	Average [c]	640 ± 10	0.3 ± 0.3	64.9 ± 0.3	0.2 ± 0.1	0.2 ± 0.2
	Best [d]	650	0.6	65.0	0.3	0.4

[a] Derived from the *J-V* curves (sweep rate 100 mV s^{-1}; short-circuit to open-circuit); V_{oc} – open-circuit voltage, J_{sc} – short-circuit current density, FF – fill factor, PCE – power conversion efficiency. [b] Quasi-stabilised power output at the potential corresponding to the maximal performance in *J-V* measurements. [c] Mean values and one standard deviation for 15 devices from 3 independent batches. [d] Data for the best-performing solar cell.

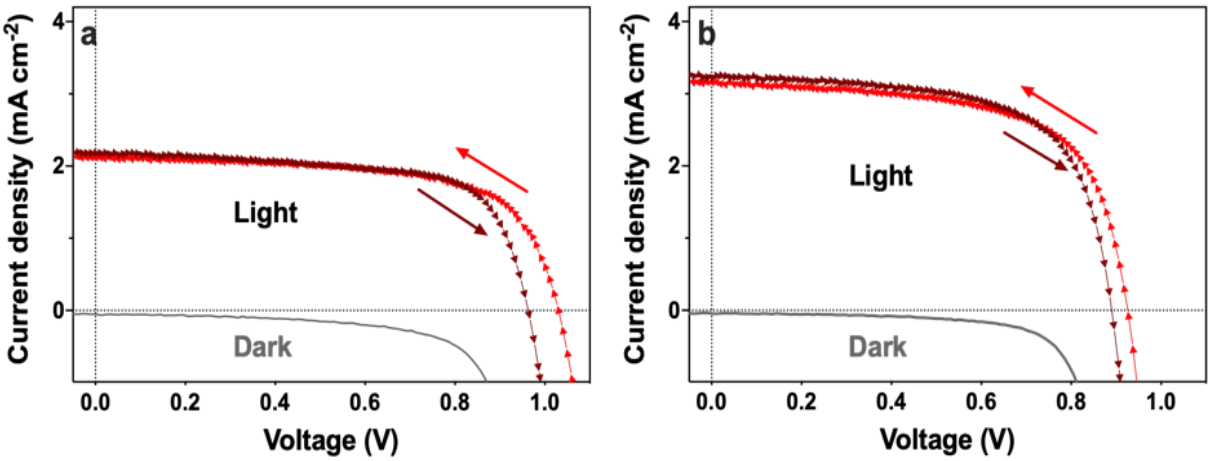

Figure S15. *J-V* curves (100 mV s^{-1}) for the Au|spiro-OMeTAD|$Cs_2AgBiBr_{6-2x}S_x$ + m-TiO_2|c-TiO_2|FTO solar cells (aperture 0.16 cm^2) measured under 1 sun AM1.5G irradiation for (a) x = 0 and (b) x = 0.10 recorded in open-circuit to short-circuit (reverse bias) and short-circuit to open-circuit (forward bias) directions (*symbols*; see arrows in the figure) and in the dark (*grey curves*).

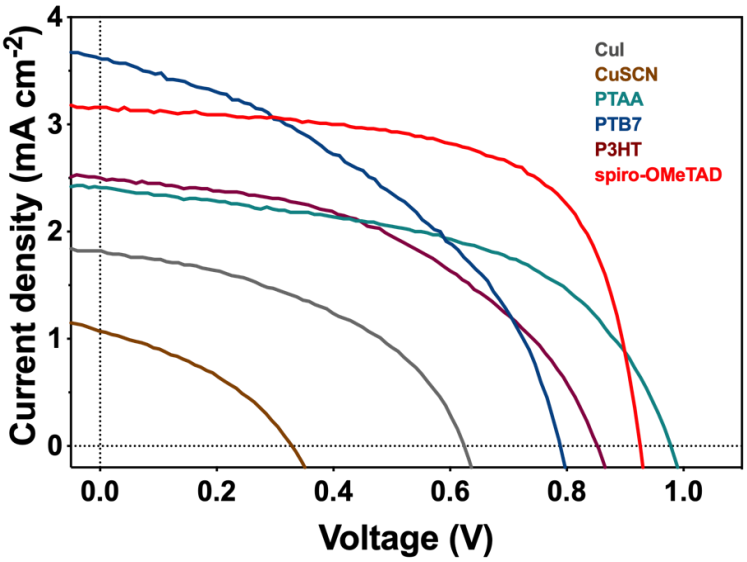

Figure S16. Effect of the hole transporting material on the *J-V* curves (100 mV s^{-1}; short-circuit to open-circuit sweeps) for the Au|HTM|$Cs_2AgBiBr_{5.8}S_{0.1}$ + m-TiO_2|c-TiO_2|FTO solar cells (aperture 0.16 cm^2) under 1 sun AM1.5G irradiation.

Table S5. Effects of the anode and HTM on the photovoltaic performance[a] of the anode|HTM|$Cs_2AgBiBr_{6-2x}S_x$ + m-TiO_2|c-TiO_2|FTO solar cells (aperture 0.16 cm^2) under 1 sun AM1.5G irradiation.

Anode|HTM	V_{oc} (mV)	J_{sc} (mA cm^{-2})	FF (%)	PCE (%)
Graphite|CuI	608 ± 10	1.4 ± 0.4	43.9 ± 0.4	0.3 ± 0.2
Graphite|CuSCN	321 ± 12	0.7 ± 0.5	37.8 ± 0.3	0.07 ± 0.05
Au|PTAA	960 ± 20	2.0 ± 0.5	52.8 ± 0.3	1.0 ± 0.2
Au|PTB7	790 ± 13	3.3 ± 0.4	41.9 ± 0.2	1.1 ± 0.1
Au|P3HT	850 ± 20	2.2 ± 0.5	46.7 ± 0.5	0.6 ± 0.4
Au|spiro-OMeTAD	910 ± 20	3.0 ± 0.3	65.0 ± 0.4	1.8 ± 0.1

[a] Parameters were derived from the *J-V* curves (sweep rate 100 mV s^{-1}) measured in the short-circuit to open-circuit direction; V_{oc} – open circuit voltage, J_{sc} – short circuit current density, FF – fill factor, PCE – power conversion efficiency.